J Appl Electrochem (2010) 40:1917–1923
DOI 10.1007/s10800-010-0177-8

ORIGINAL PAPER

Temperature dependence of morphology and oxygen reduction reaction activity for carbon-supported Pd–Co electrocatalysts

E. F. Abo Zeid · Dae-Suk Kim · Hee Soo Lee · Yong-Tae Kim

Received: 3 September 2009 / Accepted: 1 April 2010 / Published online: 24 July 2010

Abstract In this study, we investigated the heat treatment temperature effect on the morphology and oxygen reduction reaction activity of carbon-supported Pd–Co alloy electrocatalysts. As prepared Pd–Co bimetallic nanoparticles showed a single-phase face-centered cubic disordered structure, and the mean particle size decreased with a Co content. In order to improve activity and stability, the catalysts were heat-treated in a temperature range of 300 to 700 °C. From the results of oxygen reduction reaction activity tests, the optimal heat treatment temperature was found to be 700 °C for the low Co content samples, while 300 °C was the best condition for the high Co content samples.

Keywords Pd–Co nanoparticle · Oxygen reduction reaction · Electrocatalysis · PEM fuel cell · Microstructure · Nano-scale materials

1 Introduction

Polymer electrolyte membrane fuel cells (PEMFC) have been undergoing rapid development in the last few years for portable, mobile applications and in particular for the transport sector [1, 2]. PEMFCs are relatively compact, have high power density, provide rapid startup, and operate at low temperatures (60–120 °C). These characteristics make PEMFCs very attractive as a power source for vehicles compared to other fuel cell systems [3]. However, the slow kinetics of the oxygen reduction reaction (ORR) and the high cost of Pt-based electrocatalysts pose serious challenges for commercialization [4–6].

In this regard, there have been considerable efforts on the search for alternative electrocatalysts which can offer high ORR activity and good durability with the lower cost. For example, alloying Pt with less expensive metals such as Fe, Co, Ni, and Cr has drawn much attention, as they offer improved catalytic activity for ORR and durability [7, 8]. More recently, alloying Pd with other elements such as Fe, Co, and Ti has become appealing, as these elements offer high catalytic activity for ORR, and the cost of palladium is one-fifth of the cost of platinum [9, 10]. Pd-transitional metal alloys exhibited a high catalytic activity and a good selectivity for the ORR, and it might be attributed to an electronic stabilization of the added alloy element [11, 12]. In addition, Pd-based electrocatalysts with suitable metal combinations and optimum compositions exhibited high catalytic activity for the ORR; the ORR activity of the Pd–Co/C catalysts with a Co content of 10–30% was found to be close to that of Pt/C [13–15]. Also, three kinds of carbon-supported Pd-based alloy electrocatalysts, Pd–Co–Au, Pd–Co–Ti, and Pd–Co–Mo, have been prepared, and their electrocatalytic activity was found to be comparable with Pt for the ORR in a PEMFC [16].

In general, the Pt-based [17–20] and Pd-based [21–23] alloy catalysts have been prepared and/or post-treated at high temperatures in inert or reducing atmospheres in order to promote alloy formation. However, the particle size of

E. F. Abo Zeid · D.-S. Kim · Y.-T. Kim (✉)
School of Mechanical Engineering, Pusan National University, Pusan 609-735, Korea
e-mail: yongtae@pusan.ac.kr

H. S. Lee
School of Materials Science and Engineering, Pusan National University, Pusan 609-735, Korea

E. F. Abo Zeid
Physics Department, Faculty of Science, Assiut University, Assiut 71516, Egypt

Pd-based catalysts as reported in the literature [13–16] was relatively large, and thus there is a significant space to improve ORR mass activity. Challenges to be met for the preparation of improved Pd alloy catalysts include the need for synthesis procedures resulting in catalysts with desirable alloy composition, small particle size, and a narrow size distribution [24], especially for alloy electrocatalysts. Therefore, catalyst preparation methods that can offer high degree of alloy homogeneity with small particle size and high surface area at moderate temperatures are needed.

Theoretical calculations and experimental data demonstrated that, upon annealing at elevated temperatures, Pd–M alloys undergo phase segregations, in which the noble metal Pd migrates to the surface forming a pure Pd overlayer on the bulk alloys [25–27]. The electronic structures of the metal overlayers can be significantly altered upon bonding with the substrate metal and, in turn, their catalytic properties can be changed [28, 29]. Norskov et al., using their d-band center model, correlated the electronic structure of the surface metal (represented as the energy center of the valence d-band density of states) and its catalytic activity. The model has been used to explain the catalytic activity and electrochemical behavior of some strained surfaces and metal overlayers [30–33].

We present here a novel synthesis of Pd–Co/C nanoparticles by way of a modified Polyol reduction in the presence of a polycation, poly diallyldimethylammonium chloride (PDDA). In a continuing effort to improve the catalytic activity of Pd–Co alloys, we focused on the combined effect of the ethylene glycol (EG) and sodium borohydride ($NaBH_4$) as synthetic reducing agents with the presence of PDDA on catalyst morphology and on the corresponding ORR catalytic activity. The effect of heat treatment of Pd–Co electrocatalysts in the range of 300–700 °C was characterized by X-ray diffraction (XRD), transmission electron microscopy (TEM), cyclic voltammetry (CV), and ORR.

2 Experimental

2.1 Catalysts synthesis

Carbon-supported Pd_{32}–Co_{68} and Pd_{62}–Co_{38} catalysts were synthesized by a modified polyol reduction process. Pd–Co precursor solution was prepared as follows: $(NH_4)_2PdCl_4$ (Alfa Aesar Johnson Matthey Company, 99.998%) and $CoCl_2 \cdot 6H_2O$ (DAEJUNG CHEMICALS & METALS CO., LTD., 98.5%) to obtain 100 mg of Pd_{100-x}–Co_x/C were dissolved in dionized water. About 30 mL of ionic PDDA (35 wt% in water, molecular weight : about 10,000) was added to 30 mL EG (SAMCHUN PURE CHEMICAL CO., LTD., 99.5%) and sonicated for 15 min. A volume of 40 mL of EG refluxed at 130 °C under stirring, PDDA and Pd–Co precursor solution were added drop wise to the EG under stirring in 10 times with the appropriate amounts of Pd_{100-x}–Co_x to give an atomic ratio of PDDA: Pd_{100-x}–Co_x = 7:1, and an appropriate amount of carbon (Vulcan XC 72R) was added. The mixture was kept under stirring for 2 h at 130 °C. A solution containing 200 mg of $NaBH_4$ (KANTO CHEMICAL CO., INC., 92%) in 40 mL of dionized water was added under vigorous stirring, and thus the color of the solution was changed from yellow to black, indicating the processing of the reduction reactions. The mixture was kept under stirring at room temperature for overnight, and the slurry was filtered, washed with water and ethanol, and dried overnight in vacuum oven at 70 °C. These as prepared samples are denoted as Pd_{100-x}–Co_x/C–ASP. In order to study the effect of heat-treatment on the catalytic activity, the samples were heat-treated at 300 °C, 500 °C, and 700 °C in the gas mixture of 10% H_2-90% Ar for 3 h, followed by cooling to room temperature. To compare between pure Pd catalyst and Pd–Co catalyst, Pd/C was also prepared with the same procedure.

2.2 Materials characterization

Pd–Co weight percentage in the catalysts has been determined by inductively coupled plasma-atomic emission spectrometer (ICP-AES) analysis after preprocessing Pd–Co/C nanoparticles by way of a modified polyol reduction in the presence of a polycation with hydrochloric acid and nitric acid treatments.

XRD measurements of the Pd_{100-x}–Co_x/C catalysts were performed using a Philips Pan analytical X-ray diffractometer at the Korea Basic Science Institute using Cu K_α radiation ($\lambda = 0.15406$ nm). The XRD spectra were obtained using high resolution in the step-scanning mode with a narrow receiving slit (0.05°) and a counting time of 50.05 s per 0.05°. XRD patterns were recorded in the 2θ range of 10–95°. Scherrer's equation was employed to estimate particle size from XRD. For this calculation, the (111) peak of the Pd face-centered cubic (fcc)/fct structure around $2\theta = 40°$ was selected.

The morphology and particle size of electrocatalyst was observed using transmission electron microscopy (TEM, JEOL JEM-2010F). Specimens for TEM observation were prepared by placing a drop of the particle-dispersed solution onto a copper grid; then, the TEM was operated at an accelerating voltage of 200 keV. All of the images were recorded with a charge-coupled device camera.

2.3 Electrochemical measurements

Electrochemical measurements were performed on a potentiostat (Biologic VSP). Pt mesh counter electrode, a

glassy carbon (5 mm dia.) working electrode, and a reference electrode (Ag/AgCl, 3.5 M KCl) were used as a three-electrode electrochemical cell. Before each experiment, the glassy carbon electrode was polished to a mirror-like finish with 0.05 μm alumina (Buehler). The catalyst monolayer on the working electrode was prepared by dispersing 1 mg of the carbon-supported catalyst in 2 mL of dionized water, ultrasonicating until a dark homogeneous dispersion is formed, dropping 20 μL of the dispersion by micropipette onto the glassy carbon electrode. After drying for 15 min in oven at 60 °C, the catalyst monolayer was covered by dropping 20 μL of 0.025 wt% Nafion solution (Electrochem Inc.) to form a thin film on it and dried at 60 °C for 15 min in oven.

The CV was recorded in N_2-purged 0.1 M $HClO_4$ at a scan rate of 50 mV/s between –0.2 and 0.8 V (vs. Ag/AgCl). Before recording the CV, the catalyst surface was electrochemically cleaned by rapid scan rate (200 mV/s) for 50 cycles between –0.2 and 0.8 V (vs. Ag/AgCl). After CV measurements, ORR was subsequently performed in the same potential range in O_2-saturated 0.1 M $HClO_4$. The experiments were repeated at least three times to ensure repeatability of the data. All the electrochemical measurements were carried out at the room temperature.

3 Results and discussion

3.1 Structure analyses of Pd–Co/C bimetallic catalysts

Carbon-supported bimetallic Pd–Co electrocatalysts were tested to identify precise Pd–Co atomic percent through ICP-AES analysis. Ratio of Pd:Co was 32:68 and 62:38, and all of the them showed around 10 wt% of Pd–Co in the electrocatalysts.

Figure 1 compares the XRD patterns of the carbon-supported Pd–Co, (a) (Pd:Co = 32:68 atom%), (b) (Pd:Co = 62:38 atom%) prepared by a modified polyol reduction process before and after heat treatment at various temperatures. From Fig. 1a, it was observed that all of the XRD patterns exhibit five main characteristics peaks of the fcc crystalline Pd (JCPDS Card 00-005-0681) [15], namely the planes (111), (200), (220), (311), and (222) demonstrating that all the alloy catalysts mainly resemble the single-phase disordered structure (solid solution). The five diffraction peaks in the Pd–Co (32:68 atom%) alloy catalysts are shifted to higher 2θ values compared to those of Pd–Co upon heat-treatment suggesting incorporation of Co into the Pd lattice. A shift of diffraction peaks to higher angles with increasing heat-treatment temperature can be observed, indicating the contraction of the lattice and an increase in the degree of alloying of Co with Pd. The reflections correspond to only a single fcc phase suggestive of formation of a binary Pd–Co

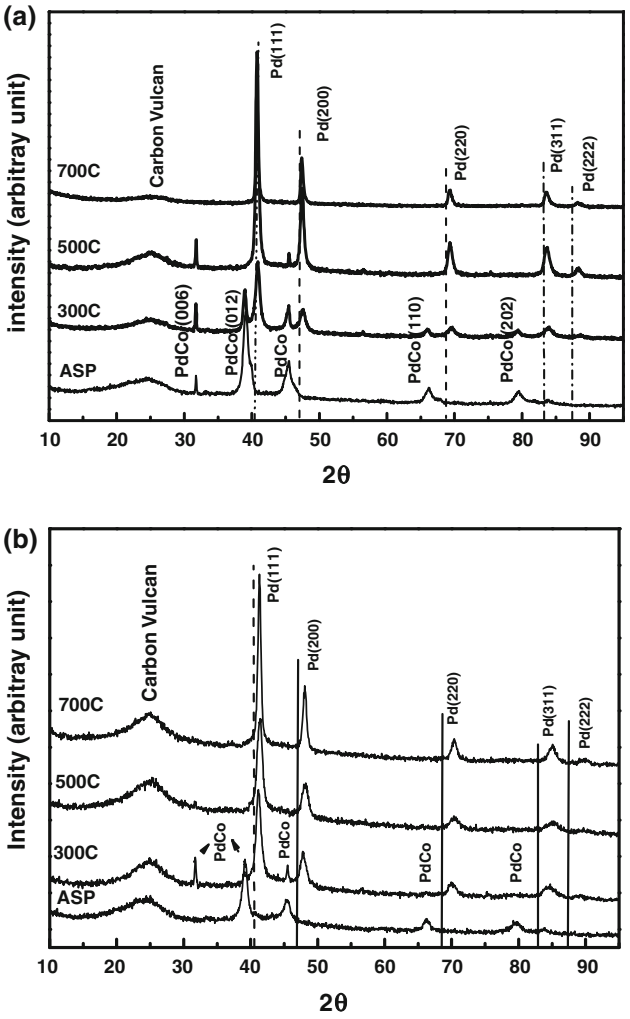

Fig. 1 X-ray diffraction patterns of carbon-supported Pd-Co. **a** Pd:Co = 32:68 atom%. **b** Pd:Co = 62:38 atom%. Catalysts prepared by a modified Polyol reduction process before and after heat treatment in 10% H_2–90% Ar atmosphere at various temperatures. The solid and dashes lines indicate standard 2θ values corresponding to the (111), (200), (220), (311), and (222) reflections of Pd metal

alloy phase. Pd–Co peak was decreased as increasing annealing temperature and finally disappeared at 700 °C heat treatment in Fig. 1a. In Fig. 1b, Pd–Co peak was completely disappeared at 500 °C, which indicating that the Pd is phase segregated during annealing at high temperature, forming a Pd-rich overlayer on the surface and this phenomenon is depended on the amount of Co portion in the Pd–Co alloy [34]. The diffraction peak at around $2\theta = 25°$ corresponds to the (0 0 2) plane diffraction of the hexagonal structure of the Vulcan-XC-72R carbon support.

The mean particle size calculated from XRD patterns for the two catalyst alloys are shown in Table 1. The particle surface area S in $m^2\ g^{-1}$ was calculated using the equation $S = 6000/d\rho$ for spherical particles [14], where d is the

Table 1 Characteristics of prepared Pd-Co/C (Pd:Co = 32:68 atom%) and (Pd:Co = 62:38 atom%) alloy catalyst by X-ray diffraction

Sample	Heat treatment	Average particle size (nm)	Active surface area ($m^2\ g^{-1}$)
Pd_{32}–Co_{68}/C	ASP	8.795	61.54
	300 °C	14.54	37.25
	500 °C	18.70	28.95
	700 °C	24.86	21.77
Pd_{62}–Co_{38}/C	ASP	10.01	54.08
	300 °C	10.09	53.66
	500 °C	10.31	52.50
	700 °C	16.85	32.11

ASP as prepared samples

crystallite size (diameter) in nm obtained from the (111) diffraction line, XRD data (Fig. 1), and ρ is the density of the Pd–Co alloy ($\sim 11.08\ g\ cm^{-3}$). This equation is obtained by dividing the surface area of a spherical particle ($4\pi r^2$) by the mass of the spherical particle (mass = density × volume = $\rho \times 4\pi r^3/3$), where r is the radius of the spherical particle ($d/2$). To make appropriate changes obtaining the surface area value in $m^2\ g^{-1}$, the density and crystal size values are substituted, respectively, in $g\ cm^{-3}$ and nm. The average particle size of Pd–Co was calculated by employing the Scherer equation $d(\text{Å}) = k\lambda/\beta \cos\theta$ [16], where d is the average particle size in Å, k is a shape-sensitive coefficient (0.9), λ is the wavelength of radiation used Cu Kα (1.54056 Å), β is the full width half maximum (in rad) of the peak and θ is the angle at the position of peak maximum (in rad). As increased the annealing temperature, the size of Pd–Co alloy was increased. The size of Pd_{32}–Co_{68}/C electrocatalyst was fast increased at the higher temperature than Pd_{62}–Co_{38}/C electrocatalyst. This means that the mean particle size was found to decrease with a decrease in Co content. Even in the high annealing temperature, the size of Pd–Co was not dramatically increased which indicates that the polyol reduction process keep from agglomerating Pd–Co catalysts at the high annealing temperature.

Pd–Co/C alloy morphology, as a function of heat treatment temperature, was recorded by TEM in Fig. 2. Before annealing Pd–Co/C catatlyst, Pd–Co alloy was agglomerated each other in Fig 2a, e. However, a uniform distribution of catalyst particles with a predominant and regular spherical shape can be observed in all samples after heat treatment at various temperatures. An increase in particle size with increasing heat-treatment temperature (Fig. 2a–h) may suggest agglomeration during heat treatment. From the images, it can be concluded that heated the catalysts are well dispersed on the carbon surface with a narrow particle size distribution. It is also observed that the average particle size is slightly higher than the untreated one and the heat-treatment appears to favor agglomeration as reported earlier [14, 17]. Therefore, the catalyst preparation procedure via a modified polyol reduction route may be a method for obtaining nano-sized alloy catalysts with a narrow particle distribution and a good dispersion on a support. It is also noted that a few larger sized particles (>50 nm) are also observed, which are formed due to aggregation of the particles at higher temperatures. This observation was also calculated from XRD data. However, the particle size of Pd–Co calculated by XRD is smaller than observed one by TEM. This means that some of the particles are likely polycrystalline. Thus, while grain–grain boundaries of the same polycrystal are not exposed, they

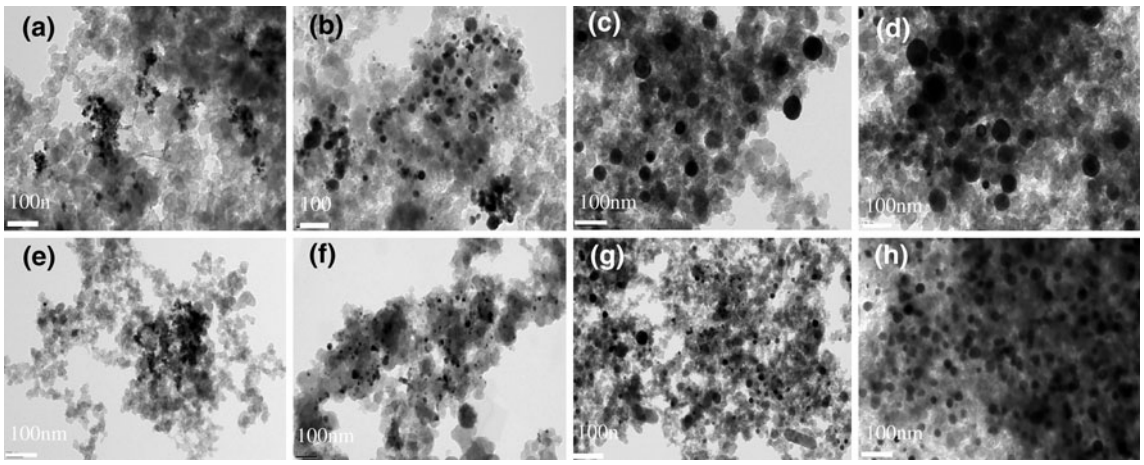

Fig. 2 Transmission electron microscopy micrographs of the carbon-supported Pd-Co (Pd:Co = 62:38 atom%) **a** ASP alloy and followed by annealing at **b** 300 °C, **c** 500 °C and **d** at 700 °C and Pd-Co (Pd:Co = 32:68 atom%) **e** ASP alloy and followed by annealing at **f** 300 °C, **g** 500 °C and **h** 700 °C

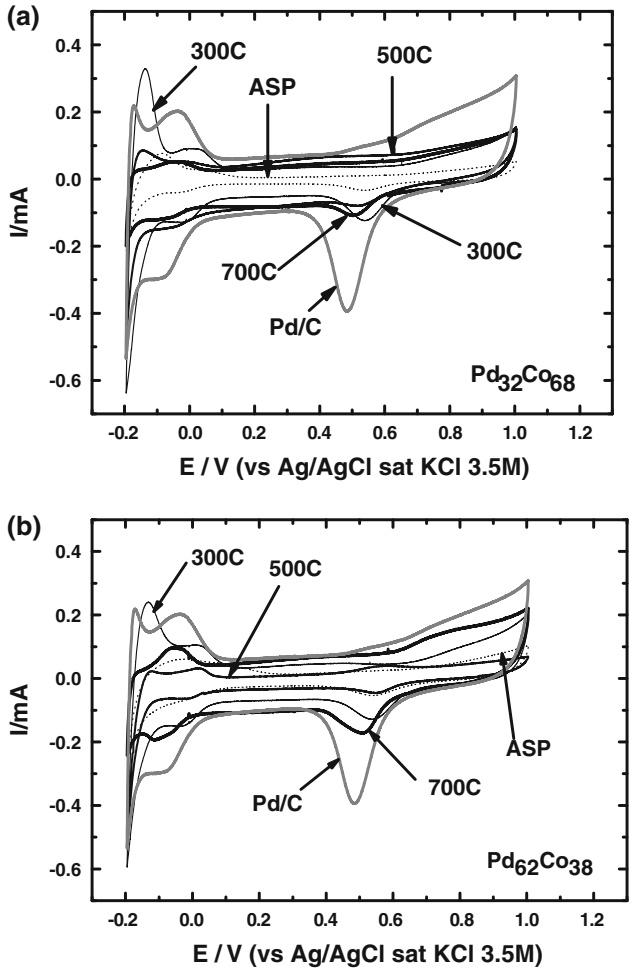

Fig. 3 Comparison of cyclic voltammograms of: **a** Pd/C ASP and Pd_{32}–Co_{68}/C and **b** Pd/C ASP and Pd_{62}–Co_{38}/C alloy catalysts synthesized by the same polyol reduction method using EG and $NaBH_4$ as reducing agents in the presence of PDDA. The Pd_{32}–Co_{68}/C and Pd_{62}–Co_{38}/C samples annealed at different temperatures, ASP, 300 °C, 500 °C and 700 °C. Recorded in a 0.1 M $HClO_4$ solutions at room temperature under O_2-free atmosphere. Potential scan rate: 50 mV s^{-1}

are included in the average size of the material determined by XRD.

3.2 Cyclic voltammograms of two Pd–Co/C alloy catalysts

CVs of the Pd/C compared with Pd–Co/C catalysts synthesized by a modified polyol reduction process using the reducing agents EG and $NaBH_4$ in the presence of ionic PDDA are shown in Fig. 3. These CVs were recorded in a 0.1 M $HClO_4$ solution under O_2-free atmosphere at room temperature. The CV of Pd–Co/C catalyst samples annealed at 300 °C and Pd/C (Fig. 3a, b) shows large peaks in the potential range of –0.192 to –0.131 V, –0.196 to –0.133 and –0.194 to -0.171, respectively, versus Ag/AgCl sat KCl 3.5 M, which correspond to the hydrogen adsorption/desorption processes. However, the other annealed samples all exhibit smaller hydrogen peaks compared to those of the 300 °C annealed sample. The peaks of the Pd/C catalyst might be due to the dissolution of adsorbed hydrogen into bulk Pd. However, in the case of Pd–Co/C annealed samples, the dissolution of hydrogen into bulk Pd–Co/C might be restrained by the existence of the second element, cobalt [12]. In the case of annealed sample (Pd_{32}–Co_{68}/C) at 300 °C, the degree of alloying for cobalt in Pd lattice forming the core shell is less than the other two annealed samples (500 °C and 700 °C). Therefore, the largest peaks of 300 °C annealed sample may be ascribed to the lower degree of alloying for cobalt in this sample than the others. Also, in the case of annealed sample at 300 °C (Pd_{62}–Co_{38}/C), it was observed that the largest peaks at 300 °C annealed sample than 500 °C and 700 °C, which confirmed that the increased degree of alloying for cobalt in Pd lattice forming the core shell at the higher temperatures increases the particle size which decreases the active surface area as indicated in XRD data. Therefore, the difference in CV shapes between the Pd/C and Pd–Co/C catalysts may reflect the difference in the Pd metal and Pd–Co/C binary alloy. Normally, the areas under the hydrogen adsorption/desorption peaks in CVs can be used to estimate the electrochemically active surface areas. However, in the case of alloy catalysts, such quantitative estimation may not be feasible. As a qualitative estimation, it can be seen that the Pd_{32}–Co_{68}/C and Pd_{62}–Co_{38}/C annealed at 300 °C sample shows the largest electrochemically active surface areas compared to the other catalyst samples, which may be due to the smaller particle size and the lower degree of the agglomeration. In addition, the onset potential for the Pd–Co oxide formation in the positive-going sweep and the oxide reduction in the negative-going sweep is slightly shifted to more positive potential for all of the Pd–Co/C catalysts as compared to Pd/C. This observation indicates that the alloying inhibited the chemisorption of oxygenated species such as OH_{ad} on the Pd sites at high potential (above 0.5 V vs. Ag/AgCl) by the change in the Pd electronic structure induced by the addition of Co. This may be beneficial to the facile oxygen adsorption at low potential, and thus the ORR kinetic enhancement.

3.3 Catalyst activity toward ORR as a function of heat treatment temperature

Figure 4 shows the ORR activity for the Pd_{32}–Co_{68}/C and Pd_{62}–Co_{38}/C alloys at different heat-treatment temperatures in an oxygen-saturated 0.1 M $HClO_4$ solution and room temperature. For comparison, we collect the ORR data at slower speed rate, 5 mV/s and high speed rate 50 mV/s. ORR curve for Pd/C was also included as a reference.

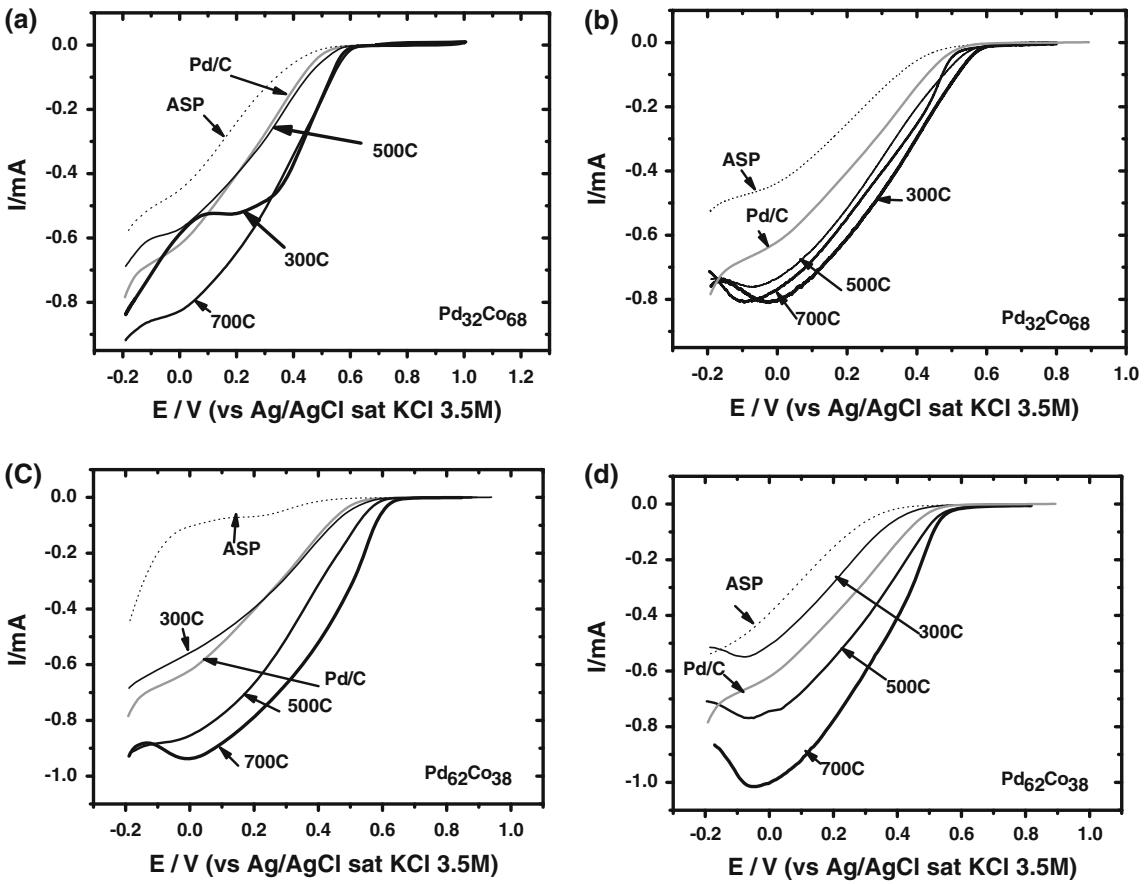

Fig. 4 Single scan voltammograms at different heat-treatment temperatures for: Pd_{32}–Co_{68}/C with the potential scan rates **a** 5 $mVs^{-1}$and **b** 50 mVs^{-1} and Pd_{62}–Co_{38}/C with the potential scan rates **c** 5 mVs^{-1} and **d** 50 mVs^{-1}, catalyst-coated GC disk electrode. Measured in an oxygen saturated 0.1 M $HClO_4$ solution at room temperature. The electrode was rotated at 1600 rpm with the negative-going sweeps. The catalyst loadings were all controlled to 12.8 μg cm^2

However, kinetic region could be only discussed among the three control regions (kinetic, mixed and diffusion limited), which is the reason why supported Pd–Co was about 10 wt%. However, through the onset potential (kinetic region), the intrinsic electrocatalytic activity could be discussed. It was observed that the high speed rates 50 mV/s have more positive onset potential than 5 mV/s. Figure 4a, b shows that the Pd_{32}–Co_{68}/C alloy electrocatalyst at 300 °C shows the highest ORR activity. The ORR activity order was from Fig. 4b as follows: Pd_{32}–Co_{68}/C (300 °C) > Pd_{32}–Co_{68}/C (700 °C) > Pd_{32}–Co_{68}/C (500 °C) > Pd/C > Pd_{32}–Co_{68}/C (ASP). The Pd_{32}–Co_{68}/C catalyst which annealed at 300 °C showed better ORR performance than those annealed at 700 °C and 500 °C, respectively. This is mainly because the catalyst which annealed at lower temperatures has a smaller particle size (larger surface area) compared to those annealed at higher temperatures catalysts. Among the Pd–Co/C alloys, the order of ORR performance is consistent with the particle size distribution order. The heat-treatment temperature from 300 °C to 700 °C causes an increase in particle size, and leads to a decrease in ORR activity of the Pd–Co/C alloy catalysts. Therefore, the heat treatment at 300 °C showed the best ORR activity.

However, Pd_{62}–Co_{38}/C catalysts showed different ORR activity compared to Pd_{32}–Co_{68}/C. The ORR activity order was from Fig. 4d as follows: Pd_{62}–Co_{38}/C (700 °C) > Pd_{62}–Co_{38}/C (500 °C) > Pd/C > Pd_{62}–Co_{38}/C (300 °C) > Pd_{62}–Co_{38}/C (ASP). This means that after high-temperature annealing, the palladium atoms tend to migrate to the surface of the alloy nanoparticles because palladium and cobalt exhibit a strong trend toward segregation due to the large segregation energy difference between them [16]. Thus, a Pd-rich "skin" should be largely formed on the Pd_{62}–Co_{38}/C catalyst than Pd_{32}–Co_{68}/C catalyst.

Therefore, Pd–Co could be segregated by heat treatment and it helped to have a Pd-rich "skin" on the surface. It helped Pd–Co/C catalyst have higher ORR activity than pure Pd/C catalyst. Especially, the optimal heat treatment temperature was found to be 700 °C for the low Co content samples, while 300 °C was the best condition for the high Co content samples. The differences in surface characteristics (e.g., crystallographic plane) and particle size

distribution depending upon the synthesis method and heating temperature influence the electrochemical activity.

4 Conclusions

Carbon-supported nano-Pd–Co/C alloy catalysts using combined reducing agents EG and $NaBH_4$ were successfully synthesized using a modified polyol reduction method. The effect of the heat treatment on the catalyst morphology and catalytic ORR activity was also examined. In order to improve activity and stability, the catalysts were heat-treated at a temperature range of 300–700 °C. Surface electrochemical measurements confirmed the formation of the Pd–Co alloy. The optimal heat-treatment temperature was found to be 700 °C for the lower concentration of Co in Pd–Co/C alloy, while 300 °C was the best condition for the high Co content. Before heat-treatment, a Pd–Co/C alloy at room temperature showed a weak ORR activity. After heat-treatment, the Pd–Co/C alloys showed enhanced ORR activity than pure Pd/C catalyst. This is because the ORR activity is dependent on the surface composition as well as the particle size. Therefore, the heat treatment condition should be individually optimized on the alloy composition.

Acknowledgments This work was supported by the Korea Research Foundation Grant funded by the Korean Government (MOEHRD) (KRF-2008-331-D00094) and a grant (M2009010025) from the Fundamental R&D Program for Core Technology of Materials funded by the Ministry of Knowledge Economy, Republic of Korea.

References

1. de las Heras N, Roberts EPL, Langton R, Hodgson DR (2009) Energy Environ Sci 2:206
2. Acres GJK (2001) J Power Sources 100:60
3. Hentall PL, Lakeman JB, Mepsted GO, Adcock PL, Moore JM (1999) J Power Sources 80:235
4. Conway BE, Bockris JO'M, Yeager E, Khan SUM, White RE (eds) (1983) Comprehensive Treatise of Electrochemistry. Springer, New York
5. Shao M, Sasaki K, Adzic R (2006) J Am Chem Soc 128:3526
6. Gasteiger HA, Kocha SS, Sompalli B, Wagner FT (2005) Appl Catal B 56:9
7. Mukerjee S, Srinivasan S, Soriaga MP, McBreen J (1995) J Electrochem Soc 142:1409
8. Stamenkovic VR, Mun BS, Mayrhofer KJJ, Ross PN, Markovic NM (2006) J Am Chem Soc 128:8813
9. Savadogo O, Lee K, Oishi K, Mitsushimas S, Kamiya N, Ota K (2004) Electrochem Commun 6:105
10. Fernandez JL, Raghuveer V, Manthiram A, Bard AJ (2005) J Am Chem Soc 127:13100
11. Lee K, Savadogo O, Ishihara A, Mitsushima S, Kamiya N, Ota K (2006) J Electrochem Soc 153:A20
12. Fernandez JL, Walsh DA, Bard AJ (2005) J Am Chem Soc 127:357
13. Savadogo O, Rodriguez FJ (2008) J New Mat Electr Sys 11:69
14. Zhang L, Lee K, Zhang J (2007) Electrochim Acta 52:3088
15. Mathiyarasuz J, Phani KLN (2007) Electrochem Soc 154:1100
16. Jiang SP, Liu Z, Tang HL, Pan M (2006) Electrochim Acta 51:5721
17. Raghuveer V, Ferreira PJ, Manthiram A (2006) Electrochem Commun 8:807
18. Adzic RR, Zhang J, Sasaki K, Vukmirovic MB, Shao M, Wang JX, Nilekar AU, Mavrikakis M, Uribe F (2007) Top Catal 46:249
19. Shao M, Liu P, Zhang J, Adzic R (2007) J Phys Chem B 111:6772
20. Di Noto V, Negro E, Gliubizzi R, Lavina S, Pace G, Gross S, Maccato C (2007) Adv Funct Mater 17:3626
21. Xiong L, Manthiram A (2004) J Mater Chem 14:1454
22. Dinoto V, Negro E, Lavina S, Gross S, Pace G (2007) Electrochim Acta 53:1604
23. Liu H, Manthiram A (2009) Energy Environ Sci 2:124
24. Raghuveer V, Manthiram A, Bard AJ (2005) J Phys Chem B 109:22909
25. Rousset JL, Bertolini JC, Miegge P (1996) Phys Rev B 53:4947
26. Bozzolo G, Noebe RD, Khalil J (2003) Appl Surf Sci 219:149
27. Liu Z, Koh S, Yu C, Strasser P (2007) Electrochem Soc 154:1192
28. Hammer B, Norskov JK (2000) Adv Catal 45:71
29. Kitchin JR, Norskov JK, Barteau MA, Chen JG (2004) J Chem Phys 120:10240
30. Xu Y, Ruban AV, Mavrikakis M (2004) J Am Chem Soc 216: 4717
31. Zhang JL, Vukmirovic MB, Xu Y, Mavrikakis M, Adzic RR (2005) Angew Chem Int Ed 44:2132
32. Kibler LA, El-Aziz AM, Hoyer R, Kolb DM (2005) Angew Chem Int Ed 44:2080
33. Stamenkovic V, Mun BS, Mayrhofer KJJ, Ross PN, Markovic NM, Rossmeisl J, Greeley J, Norskov JK (2006) Angew Chem Int Ed 45:2897
34. Shao MH, Huang T, Liu P, Zhang J, Sasaki K, Vukmirovic MB, Adzic RR (2006) Langmuir 22:10413